UPGRADE OF A RAMAN SPECTROMETER WITH MODERN COMPUTER CONTROL AND DATA ACQUISITION FOR STUDIES OF HYDROGEN BONDING IN PYRIMIDINE

by

Austin Archie Howard

A thesis submitted to the faculty of the University of Mississippi in partial fulfillment of the requirements of the Sally McDonnell Barksdale Honors College

Oxford
May 2009

Approved by

_____
Advisor: Professor Nathan Hammer

_____
Reader: Professor Gregory Tschumper

_____
Reader: Professor Susan Pedigo

ACKNOWLEDGEMENTS

ABSTRACT

AUSTIN ARCHIE HOWARD: Upgrade of a Raman Spectrometer with Modern
Computer Control and Data Acquisition for Studies of Hydrogen Bonding in Pyrimidine
(Under the direction of Dr. Nathan Hammer)

The restoration of a Cold War era high resolution Raman spectrometer to working order as well as its control and data acquisition upgrade using a Labview program authored for this purpose are discussed. The restored Raman spectrometer was used in an investigation of intermolecular interactions involving pyrimidine. Following in this manuscript are three chapters. The first chapter is a brief description of the history and theory of Raman spectroscopy as well as some details of the instrumentation used in Raman spectroscopy. The second chapter contains technical details of the restoration and upgrade of the high resolution Raman spectrometer. The third chapter contains data and analysis for the investigation of intermolecular interactions involving pyrimidine, including the investigation of weak hydrogen bonds by Raman spectroscopy of liquid and crystalline pyrimidine at varying pressures up to 30000 psi and strong hydrogen bonds in binary mixtures of pyrimidine and seven different molecules. The position of the ν_1 peak in the Raman spectrum corresponding to pyrimidine's ring-breathing mode was used as the marker to monitor the degree of hydrogen bonding and species involved. For mixtures of water, other peaks in the Raman spectrum were found to shift as well when the concentration of water is increased.

TABLE OF CONTENTS

1 History, Theory, and Instrumentation

Spectroscopy is the study of the interaction of light and matter.[1] The measurement of this interaction can reveal a wide range of chemical and physical behavior in systems being studied. Raman spectroscopy exploits the Raman Effect, the inelastic scattering of light by molecules. Following is a brief introduction to the interaction of light and matter, first with a description of light scattering and then with a description of the Raman Effect and its relationship to the vibrational energy of molecules. This background information precedes a short history of Raman instrumentation containing pertinent technical details.

1.1 Light-Matter Interaction

When light is incident on an atom or molecule, there are two possibilities for interaction. First, a photon with an energy exactly matching that of a vibrational, electronic, or rotational energy level transition can be absorbed by the atom or molecule. This absorption promotes the system to a higher energy level. For photons not of the correct energy to be absorbed, scattering can occur. The elastic scattering of photons was described in the 19th century, an effect now known as *Rayleigh scattering.*[2] Lord Rayleigh showed the relationship between scattering power and wavelength and why this causes the blue color of the sky. Rayleigh scattering occurs by a process in which the

oscillating electric field of light incident on a molecule induces a dipole moment in the molecule by separating positive and negative charge density. Because the electric field oscillates sinusoidally, the induced dipole moment oscillates with the same frequency. Since electric dipoles produce electric fields, this dipole oscillation produces a new electric field oscillating with the same frequency as the incident light. Oscillating electric fields induce oscillating magnetic fields, and thus new light of the same frequency as the incident light has been produced, emanating in all directions from the molecule. This scattering process is termed *elastic* because the energy of the incident light is equal to the energy of the scattered light following from the fact that energy is related to frequency by Planck's constant (Eqn. 1).

$$\varepsilon = hf \tag{1}$$

We can imagine this process with a classical picture of the oscillating dipole described above. In a linear dielectric material, the magnitude of an induced dipole is given by Equation 2.

$$p = \alpha E \tag{2}$$

In Equation 2, p represents the magnitude of the induced dipole, α is the polarizability of the material, and E is the magnitude of the electric field responsible for the induced dipole. For electromagnetic radiation, we know that the electric field has the form $E = E_o \cos \omega t$ where E_o is the magnitude of the electric field, ω is the angular frequency (the frequency f in hertz multiplied by 2π), and t is the time. It is trivial, then, to substitute the correct form of the electric field in an incident light wave into Equation 2 to obtain Equation 3, an expression for the frequency of the oscillating dipole when light undergoes Rayleigh scattering.

$$p = \alpha E_o \cos \omega t \qquad\qquad (3)$$

When a photon is inelastically scattered (Raman scattered), the scattered radiation has a different energy and thus frequency than the incident radiation. Inelastic scattering of photons was first discovered in 1923 when Arthur Holly Compton found that X-rays were shifted to longer wavelengths in collisions with electrons.[3] In 1923, while investigating theoretically the dispersion of electromagnetic radiation using a quantum model of light, Adolf Smekal showed that scattered monochromatic light would have components at higher and lower frequencies in addition to the elastically scattered component, thus theoretically predicting inelastic scattering. However, this and other contributions to the discussion of dispersion at the time did not influence C.V. Raman in his work.[4] Raman had been investigating the scattering of light since the early 1920's in order to disprove Rayleigh's idea that the blue appearance of the sea was due only to the reflection of the sky.[4] Raman was also led by similar interests to experimentally investigate how light is scattered in liquids and crystals. Raman's discovery of the effect now bearing his name took place during his attempts to find the optical analog of the Compton scattering of X-rays.[4]

Raman's setup used a telescope to focus sunlight onto various samples. A colored filter was used to illuminate the samples with monochromatic light, and a spectroscope was used to visually detect a change in the color of the scattered radiation. The effect was first termed by Raman and his assistants a "feeble fluorescence," referring to an optical process resulting from electronic relaxation, but a change in polarization of the scattered light distinguished this effect from fluorescence.[3] The effect was very weak (approximately 1 in 10^8 photons are scattered this way), but using long exposure times,

Raman was able to collect the spectra (on photographic plates in those days) of sixty different liquids and vapors. These spectra first appeared in the *Indian Journal of Physics*[5] along with his articles. Because *Nature*[6,7] had not published Raman's spectra with his articles, he sent copies of the *Indian Journal of Physics* paper to two thousand scientists in France, Germany, Russian, Canada, and the United States.[4] Raman realized as others did that the spacing of the lines in spectra he collected was equal to the infrared frequencies of the molecules represented by the spectra.[4] The terms *Raman Effect* and *Raman lines* were coined by 1929,[4] and physicists and chemists all over the world began to collect Raman spectra to investigate the vibration and rotation of molecules and verify quantum theories.[3]

1.2 The Raman Effect

A simplified explanation of the Raman Effect and its relation to molecular vibrations follows. According to Equation 2 above, the induced dipole moment in a molecule is equal to the product of the polarizability and the applied electric field. Molecules are constantly vibrating at any temperature above 0 K. For a homonuclear diatomic molecule, we can write the nuclear displacement from the equilibrium position as Equation 4.

$$q = q_o \cos \omega_v t \qquad (4)$$

Equation 4 is a result of modeling the two atoms as two masses connected by a spring. That is, the atoms are subject to a restoring force directly proportional to displacement from equilibrium. Here, ω_v is the angular frequency of the vibration. These vibrations

cause a change in electron density, and as a result, the polarizability is not accurately represented by a static variable but as a function of nuclear position (Equation 5).

$$\alpha = \alpha_o + \left(\frac{\partial \alpha}{\partial q}\right)_o q_o + \cdots \tag{5}$$

This series can be truncated at the term linear in q_o for small amplitudes of vibration. Now, Equation 3 can be written with Equation 5 substituted for the polarizability.

$$p = \alpha_o E_o \cos \omega t + \left(\frac{\partial \alpha}{\partial q}\right)_o q E_o \cos \omega t \tag{6}$$

Now, we substitute the expression for q (Equation 4).

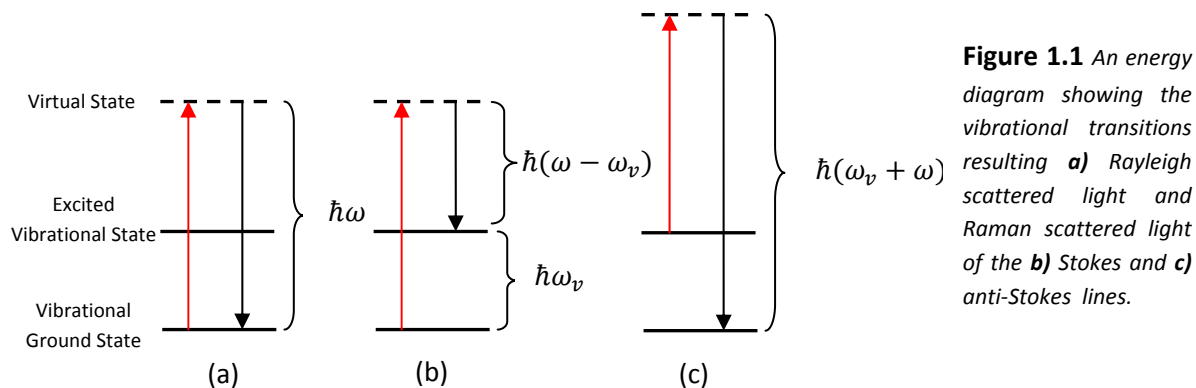$$p = \alpha_o E_o \cos \omega t + \left(\frac{\partial \alpha}{\partial q}\right)_o q_o E_o \cos \omega t \cos \omega_v t \tag{7}$$

Lastly, applying the trigonometric identity $\cos a \cos b = \frac{1}{2}[\cos(a + b) + \cos(a - b)]$, we obtain a classical theory describing Raman scattered light.

$$p = \alpha_o E_o \cos \omega t + \frac{1}{2}\left(\frac{\partial \alpha}{\partial q}\right)_o q_o E_o \{\cos[(\omega + \omega_v)\, t]$$
$$+ \cos[(\omega - \omega_v)t]\} \tag{8}$$

We can see from the above equation that the dipole induced by light interacting with the vibrating diatomic molecule is oscillating with frequency ω, the frequency of the incident radiation corresponding to the Rayleigh scattered light. Also, the dipole contains components oscillating with frequencies $\omega+\omega_v$ and $\omega-\omega_v$. The result is that the induced dipole is emitting light with frequencies greater than or less than the incident light by an amount equal to the frequency of vibration. An energy level diagram for each situation is shown in Figure 1.1.

Figure 1.1 *An energy diagram showing the vibrational transitions resulting **a)** Rayleigh scattered light and Raman scattered light of the **b)** Stokes and **c)** anti-Stokes lines.*

When light is Rayleigh scattered, the molecule is excited to a virtual excited state and relaxes, creating a photon of the same frequency. Light may also be Raman scattered as shown in Figure 1.1b and Figure 1.1c. Figure 1.1b represents the *Stokes line*. The molecule is excited to a virtual state of energy $\hbar\omega$. The molecule then relaxes to a vibrational excited state of energy $\hbar\omega_v$. The photon created in this case has energy less than the exciting radiation by an amount $\hbar\omega_v$. This is the property that makes Raman spectroscopy such a valuable tool. By measuring the intensity of scattered light over a range of frequencies, the frequencies observed to have intense emissions correspond to $\hbar(\omega - \omega_v)$. Thus, the frequency of the monochromatic exciting radiation can be used to find vibrational frequencies of the molecule. The transition producing the anti-Stokes line corresponds to a molecule in a vibrational *excited* state being excited to a virtual state and relaxing to the vibrational *ground* state. The frequency of this scattered radiation is greater than that of the excited radiation and can give similar information about vibrational frequencies. In practice, Raman spectroscopy measures Stokes lines more often because of the fact that at room temperature the vast majority of molecules will be

in the vibrational ground state. With more molecules to produce them, the Stokes lines will be more intense. It is worth noting that *Stokes* and *anti-Stokes lines* are terms originating in fluorescence spectroscopy. A fluorescence peak is predicted to be at a lower energy than the exciting radiation producing the fluorescence and is said to have *Stokes-shifted*. This process is wholly unrelated to the Stokes lines produced by the Raman Effect, and the use of these terms has simply carried over from fluorescence spectroscopy.

This above situation was described for a homonuclear diatomic molecule for simplicity. For a general polyatomic molecule, the case becomes more complicated. The vibrations are not just stretching or contraction of one bond but can be any linear combination of what are known as normal modes. The term *normal mode* when applied to molecular vibrations is characterized by the fact that each atom executes simple harmonic motion with the same frequency, and the atoms generally move in phase.[8] *Normal* refers to the fact that the displacements of one atom during any two different normal modes are orthogonal, i.e. have an inner product of zero. For a molecule of N atoms, there exist $3N$-6 normal modes (or $3N$-5 for a linear molecule). This number corresponds to three degrees of freedom of motion for each atom (i.e. in the x, y, and z directions) with the number of motions corresponding to rotation and translation of the molecule subtracted.   As noted above, any motion of the atoms of a molecule can be represented by an equation of motion that is nothing more than a linear combination of the normal mode equations of motion. Each normal mode has an energy associated with it, although the energy may be the same for two normal modes. The predicted energy for a normal mode and often its symmetry properties are used to assign the peaks in a Raman

spectrum to particular normal modes. Not every normal mode will have a peak present in the Raman spectrum, however. As noted, two normal modes may have the same energy and then are said to be degenerate. These normal modes will not be distinguishable in a Raman spectrum. In addition, certain normal modes are not *Raman active*. Notice the second term in Equation 8 containing the derivative $\left(\frac{\partial \alpha}{\partial q}\right)_o$ as a coefficient. If this derivative is zero, the dipole will not have components oscillating at either of the Raman shifted frequencies, at least to first order. Thus, no Raman scattered light will appear. Physically, we interpret this as a change in polarization with a normal mode being a requirement for that mode's Raman activity. In moving from the homonuclear diatomic case to the general polyatomic case, the induced dipole and the electric field must be represented as three dimensional vectors. The polarizability in this case must be represented as a rank two tensor in three dimensions. Only one component of the polarizability tensor must change during a normal mode for this mode to be Raman active. Typically, modes are determined to be Raman active or inactive using symmetry considerations of the mode and of the polarizability tensor for a certain point group. One advantage of Raman spectroscopy is that some vibrational modes that are not infrared active may be Raman active.

1.3 Instrumentation

Raman first used sunlight focused by a telescope as the exciting source in his experiments along with colored filters and the human eye for detection of the effect now bearing his name. Raman first collected spectra using a mercury lamp as the source, a prism to disperse the scattered radiation, and photographic plates as the detectors. The Raman

Effect, as noted above, is very weak, and as a result, collection spectra using mercury lamps and photographic plates required long exposure times (on the order of 180 hours for vapor samples, for example[4]). In these early days, however, Raman spectroscopy was still relatively easier than infrared spectroscopy and was therefore a field with much activity.[9] Raman spectroscopy still presented many challenges, however. The weak signal resulting from inelastically s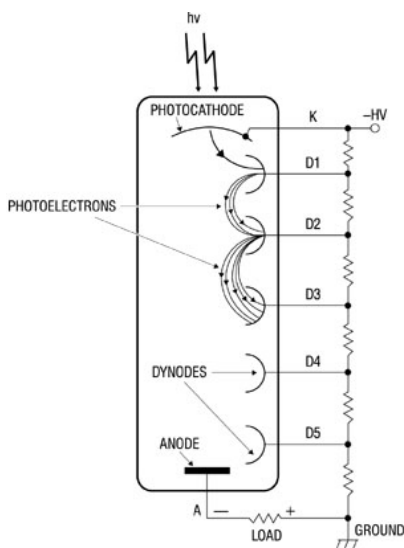cattered light was difficult to detect over the elastically scattered light from the source. Problems with fluorescence and stray light were avoided by extensively purifying liquid samples, for example, with multiple distillations that required as much as three months preparation time.[9] Problems of stray light and fluorescence became insurmountable obstacles to Raman spectroscopy of polycrystalline materials. Advances in technology through the 1950s, 1960s, and 1970s removed the challenges presented by collecting high

Figure 1.2 *Principles of a photomultiplier tube*

quality Raman spectra. The photomultiplier tube (Figure 1.2)[10] was invented for astronomers to detect low intensity light and by the 1950s had been incorporated into Raman spectroscopy setups. The photomultiplier tube is capable of detecting single photons. Photons strike a photosensitive material held at high negative voltage (~ -1500V, e.g.) and cause the emission of electrons via the photoelectric effect. The photomultiplier is made up of a number of other *dynodes*, which are conducting plates each held at increasing positive voltage by means of a voltage divider circuit. Electrons emitted at the photocathode are accelerated toward the first dynode because of the

increasing potential. The impact of these electrons then causes emission of even more electrons from the dynode, and the cascade of electrons continues until, at the last dynode, the number of electrons corresponding to a single photon is greatly increased. Electrons strike the anode and create electrical pulses that are amplified and sent to a counter. The number of counts is directly proportional to the intensity of the light striking the photocathode and is therefore a measure of signal intensity. So-called *dark counts* resulting from emission of electrons without any incident light are minimized by cooling the photomultiplier tube.

There were other technological advances that improved Raman sources and optics. The laser was first used as a Raman source in 1964 to study materials in the gas phase. Lasers were ideal for Raman excitations because they were both very intense and monochromatic. Diffraction gratings began to replace prisms as the dispersive elements in Raman spectroscopy as they became commercially available by the 1950s.[11] Gratings disperse light using destructive interference. Each wavelength of light constructively interferes at a certain angle relative to the normal of the grating with all the others interfering destructively. Therefore, by turning the grating while keeping Raman scattered light incident at a constant angle or alternatively by moving the detection slit, the intensity of light can be measured at different wavelengths with very high resolution. The first gratings were produced by machines carving slits into the surface of the grating. Ruled diffraction gratings offer several advantages to prisms as dispersive elements. Prisms are more expensive to produce than gratings and must be made of different materials depending on the wavelength region in which they are to be used.[12] Gratings, on the other hand, can be used to disperse any wavelength of light. Also, gratings

disperse light linearly, unlike prisms. In the 1960s *interference* or *holographic* gratings were first developed. These gratings are produced by an interference pattern of an intense light source varying sinusoidally in intensity along the surface of a photosensitive material. The degraded portion of the material is then dissolved, producing grooves in a sinusoidal pattern on the grating. Holographic gratings began to be produced commercially in 1972 and hold many advantages over mechanically ruled gratings in Raman spectroscopy. Flaws in the rulings of a mechanical grating resulting from carving one groove at a time are virtually nonexistent in holographic gratings, in which all the grooves are formed simultaneously. Holographic gratings also reduce the amount of stray light resulting from scattering by the grating itself.[11] By the 1970s Raman spectrometers were commercially sold with multiple holographic gratings that could record spectra within 5 cm^{-1} of the Rayleigh scattered light of the laser.[9]

The next major advances in Raman spectroscopy instrumentation were in the form of detectors. The photomultiplier tube offered advantages with its high signal-to-noise ratio and high sensitivity. However, acquiring spectra was still a lengthy process. A Raman spectrometer employing diffraction gratings and a photomultiplier tube has to collect one data point at time. That is, the photon counter must record data with the diffraction grating at one position and then turn the grating by a small amount before acquiring more data. Slow scans over a range of 3000 cm^{-1} or more would take hours. In addition, the time required must be multiplied if multiple spectra are to be collected and averaged for signal to noise enhancement. This meant that any system stable for only short amounts of time could not be studied directly by Raman spectroscopy. Furthermore, Raman spectroscopy could not be used as a way to monitor a system's

evolution in time because of the scanning time required. These problems were addressed when multichannel detectors, the "digital analog of photographic plates,"[9] were invented. Although photographic plates measure an entire spectrum simultaneously, the process is not quick, as plates must be exposed for long amounts of time and then developed. Modern multichannel detectors use an array of photosensitive elements containing electronic circuitry to detect light. In a photodiode array (PDA), photodiodes are arranged linearly and are placed in the plane of dispersed light. The light incident on an individual photodiode causes a buildup of charge that can be measured and read by a computer. Calibration of the photodiode array allows regions of the spectrum to be assigned to the individual photodiodes so that the charge accumulated on the photodiodes can produce a spectrum. Charge-coupled devices (CCD), another type of modern Raman detector, have a two dimensional array of photosensitive elements that work similarly to photodiode arrays. Multichannel detectors offer high acquisition speed and thus the ability to perform many scans in a short amount of time, drastically reducing the signal-to-noise ratio of the spectrum. Multichannel detectors also allow time resolved studies. Since the time required to acquire one Raman spectrum is so short, many can be collected over a period of time and used to study how a system evolves. Despite the advantages of CCD and PDA detectors, photomultiplier tubes still offer much higher sensitivity than their more modern counterparts. Because of the size of the array of photosensitive elements limits the amount to which light can be dispersed and still detected over a suitable range, photomultiplier tubes are also capable of acquiring spectra with higher resolution.

1.4 References

(1)   McHale, J. L. *Molecular Spectroscopy*, **1999**.

(2)   Hecht, E. *Optics*; Second ed.; Addison, **1987**.

(3)   Chodos, A. In *APS News* **2009**; Vol. 18.

(4)   Singh, R. *Physics in Perspective* **2002**, 399.

(5)   Raman, C. V. *Indian Journal of Physics* **1928**, *2*, 388.

(6)   Raman, C. V. *Nature* **1928**, 619.

(7)   Raman, C. V. *Nature* **1928**, 501.

(8)   Herzberg, G. *Infrared and Raman Spectra*; Van Nostrand Reinhold: New York, **1945**.

(9)   Adar, F.; Delhaye, M.; DaSilva, E. In *Waters Symposium, Pittcon* **2003**.

(10)   In *Laser/Electro-Optics Technology Series*; Bateman, G., Ed. **1997**.

(11)   Palmer, C. *Diffraction Grating Handbook*; 6th ed., **2005**.

(12)   Skoog, D. A.; Holler, F. J.; Crouch, S. R. *Principles of Instrumental Analysis*; Sixth ed.; Thomson, **2007**.

2 Upgrade of a High Resolution Cold War Era Raman Spectrometer for Modern Data Acquisition and Control

In Chapter 1, the theory, history, and instrumentation of Raman spectroscopy were presented. Following below are the details of the implementation of a Raman spectroscopy experimental setup using a high resolution spectrometer manufactured during the 1970's updated with modern computer control and data acquisition.

2.1 Ramanor HG2-S Raman Spectrometer

By 1972, Jobin-Yvon, a French photonics company that had produced the first commercially available holographic diffraction gratings, was offering Raman spectrometers equipped with a double monochromator and a photomultiplier tube detector. The user's manual accompanying this instrument billed the Ramanor HG2-S as "the first to take full advantage of the unique properties" of holographic gratings. Their monochromator design was reduced to a single dispersing element, the "Concave Aberration Corrected Holographic Grating." This differs from other instruments that use prisms and gratings in tandem (more dispersing elements tend to produce more stray radiation). According to the user's manual, the HG2-S contains a monochromator

comparable in efficiency to a triple grating instrument being able to record Raman lines within 4 cm^{-1} of the laser line. An optical diagram of the instrument reproduced from the original user's manual is shown below in Figure 2.1.   Scattered light is emitted from the sample and is focused onto the first mirror M1. M1 directs light through the first slit. All
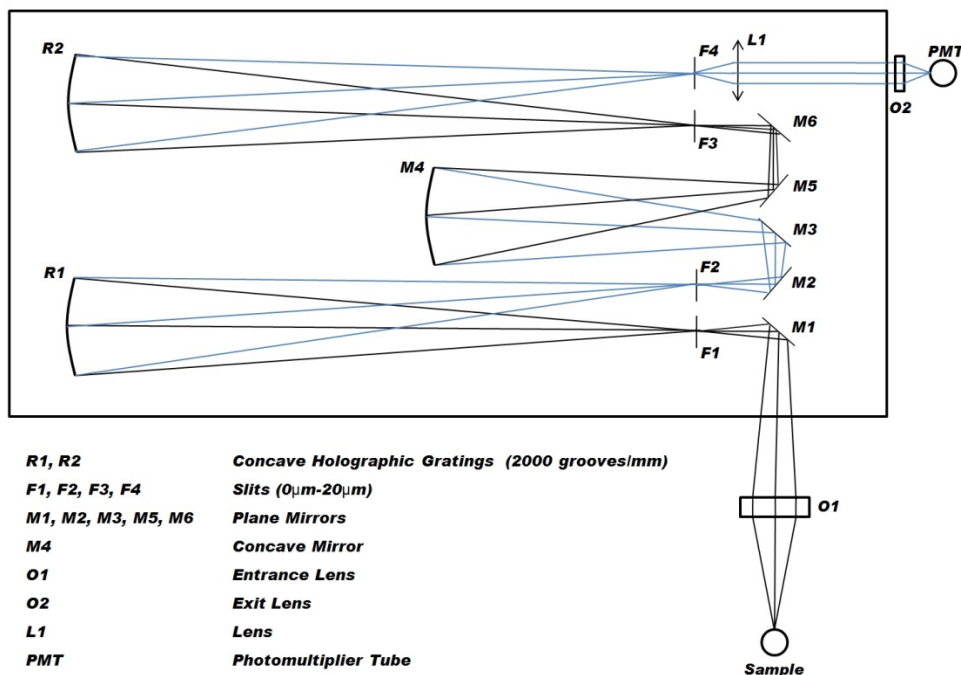

R1, R2	Concave Holographic Gratings (2000 grooves/mm)
F1, F2, F3, F4	Slits (0μm-20μm)
M1, M2, M3, M5, M6	Plane Mirrors
M4	Concave Mirror
O1	Entrance Lens
O2	Exit Lens
L1	Lens
PMT	Photomultiplier Tube

Figure 2.1 *Optical diagram of Ramanor HG2-S Raman spectrometer with explanations.   Note that additional optics allowing a single monochromator option have been omitted.*

four slits in the Ramanor are stepping motor-controlled and can be set to widths between 0μm and 20μm in steps of 0.01μm. The light from slit one is dispersed by the first concave holographic grating and directed through F2. The light then passes through the second monochromator, equipped as the first with two slits and a concave holographic grating.   The two monochromators are joined by a concave mirror labeled M4 in the diagram. The dispersed Raman scattered light is focused onto the photomultiplier tube by two lenses. Scans are carried out by rotating the two gratings about an axis parallel to the page via a stepping motor. The opening of the slits is parallel to the rotation axis of the gratings.   This arrangement of slits and gratings is known as the Littrow

configuration. The Ramanor is equipped with optics on a platform that can be lowered into position to divert the light between M5 and M6 directly to the photomultiplier tube. This option allows the Ramanor to be used as if it were equipped with a single monochromator. These optics are not shown in the optical diagram in Figure 2.1. Photographs of the optics pictured in Figure 2.1 are shown in Figure 2.2 and Figure 2.3 below.
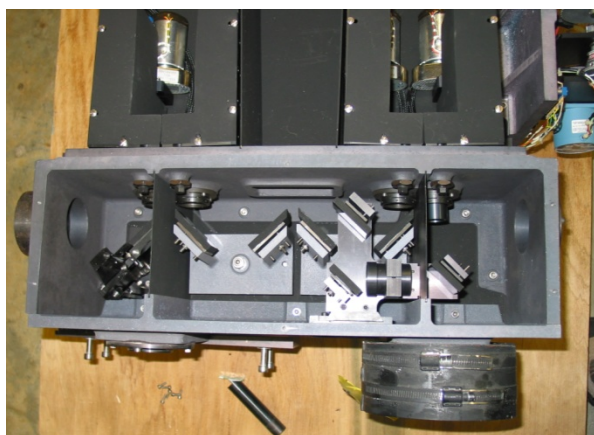

Figure 2.2 *The plane mirrors of the Ramanor. A sample is placed outside the outlet on the left.*
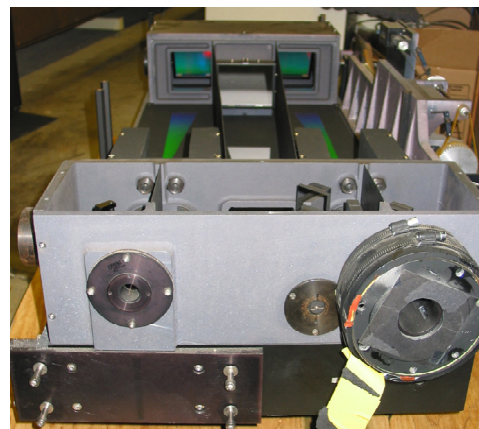

Figure 2.3 *The monochromators of the Ramanor. The camera's flash is being dispersed in the photograph. The concave mirror is between the two gratings.*

The monochromator was originally controlled by an electronic rack that allowed users to control wavenumber position, scan speed, and slit width. Spectra were acquired manually or using a device that allowed automation of spectral acquisition known as the Ramandigit 03. The original operations manual contains serial connection pin assignments and necessary commands to fully automate scanning using a computer either with or without the Ramandigit 03. The Ramandigit 03 provided a digital display of current wavenumber position and offered different scanning or recording modes. In 1987, a group of scientists from the Oak Ridge Gaseous Diffusion Plant in Oak Ridge,

Tennessee, and the University of Tennessee in Knoxville, Tennessee, found it necessary to update the computer-control system in place on a Ramanor HG2-S.[1] While spectra were originally obtained from the Ramanor by means of a line printer reading the amplified photomultiplier tube signal, the computer-control system being updated by these scientists was already capable of controlling the monochromator and of data collection and storage. According to the introduction of Ref. 1, the authors sought to update the computer-control system of this spectrometer because of the "disappointing performance of the vendor-supplied computer." They found that their experimental setup was not optimized to their needs because of "unreliable operation and unsuitable software." They set out to acquire a set of basic operating programs that they could edit themselves to fit their specific needs. They reasoned that this would allow them sufficient customization of their setup without the amount of time and effort required to compose their own software entirely. The authors found a set of programs on a Digital Equipment Corporation PDP 11/23 computer running the Raman spectrometer at the University of Tennessee Chemistry Department. The authors acquired their own DEC computer and modified the programs accordingly to implement them in their own experimental setup. A block diagram of their experimental setup is shown below Figure 2.4. The diagram shows the Ramanor spectrometer equipped with a sample compartment, an optional feature provided by Jobin-Yvon, and a microscope for acquiring Raman spectra of microscopic samples. The diagram also shows their photomultiplier tube detector and its housing, cooled by water bath at 10°C and cooled further thermoelectrically to temperatures in the range between -20°C and -30°C. The cathode of the photomultiplier tube is held at -1500V by an Ortec high voltage power

supply. The output of the photomultiplier tube at the anode is passed through an amplifier/discriminator which amplifies only pulses above a certain threshold to reduce spectra noise. The slit control pictured is the same electronic rack from the original setup mentioned above. The spectrometer, with the exception of the slits, is controlled by the computer through the Spectra Link interface. The Spectra Link
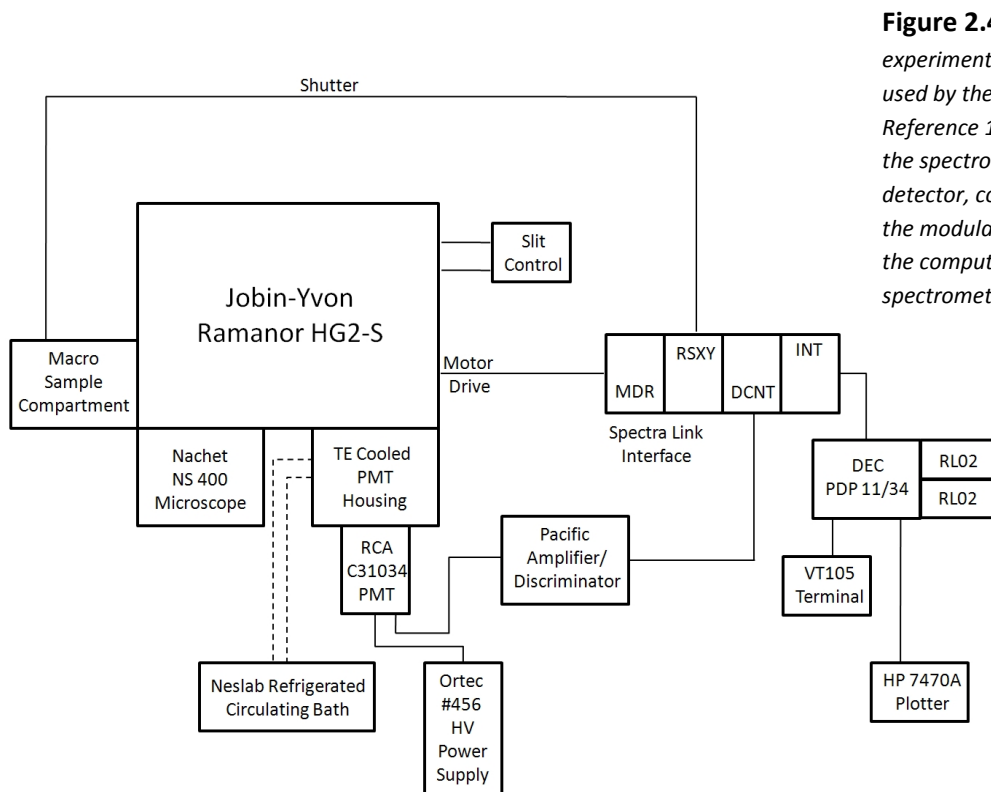

Figure 2.4 *The experimental setup used by the authors of Reference 1 showing the spectrometer, detector, computer, and the modular interface of the computer and the spectrometer*

interface was a scan and data acquisition system that used different modules programmed and called by means of DIP switches on each module. Many modules were available so that experimental setups could be customized to fit any experimental needs. This setup used the motor driver module (MDR) to drive the stepping motor controlling the monochromators, the recorder/shutter module (RSXY) to block the laser from entering the sample compartment, the pulse count module (DCNT) to read pulses from the amplifier/discriminator thus counting photons, and the interface module (INT) to link the

other modules to the computer. Their report on updating the spectrometer goes into great detail regarding the intricacies involved in interfacing the software and hardware of this setup and in the routines this setup can execute to automate spectral acquisition. The result of their work was a "more reliable, more flexible, larger, easier to use" system, "compatible with laboratory equipment and independent from restrictive operating systems."

2.2 The Restoration

By 2007, the spectrometer described above had been placed in storage at the University of Tennessee along with many of the components from the experimental setup described in Figure 2.4. In the fall of 2007, the Hammer group at the University of Mississippi acquired the Raman spectrometer and all pieces of equipment that the senders thought to be relevant, including the Spectra Link. In addition, the Hammer group was able to acquire copies of the original owner's manuals for the spectrometer itself from and the Spectra Link interface from Jobin-Yvon. In late 2007, our group began our attempt to restore the spectrometer to working order and update it once again with a modern computer-controlled system for running the spectrometer and taking data. The first step was to see if the spectrometer was still in working order, starting with the stepping motor that controls the monochromators. Included in a NIM (for Nuclear Instrumentation Module, a standard in electronics bins) bin filled with electronic equipment was the original rack that controlled slit width on the spectrometer in addition to an optional method for turning the diffraction gratings inside the Ramanor. The rack was still capable of controlling slit width but not grating position. We next turned to the Spectra

Link manual and tried to see what was necessary to connect the Spectra Link to the spectrometer and also to control the spectrometer. Dismantling of the Spectra Link revealed that the original modules discussed in the owner's manual were no longer present. Essentially, the Spectra Link was a box full of electronics which would not be useful, as their function and operating instructions could not be known. It is unclear whether or not the Spectra Link had these modules removed after it was no longer in use or if the modules had been replaced since the initial computer-control upgrade discussed above. In any case, a stepper motor controller had to be purchased if any attempts to turn the gratings were to be made. Sales representatives at Danaher Motion assured us that one of their controllers could be used and connected easily, as their parent company Superior Electric had invented stepping motors. The SLO-SYN WARPDRIVE SS2000D6i is a programmable motor controller and therefore best fit our needs. The motor controller is controlled by the user via included computer software, the motion controller programming interface (MCPI). The MCPI allows the user to write a routine for the stepping motor in a language based on BASIC (MC-BASIC for Motion Control BASIC) or to type the necessary commands directly into a terminal prompt. Connecting the motor to the controller presented no real challenges, as Superior Electric had not changed the color codes or pin assignments for their motors or controllers in the last thirty years. The controller was connected to the stepping motor via the same RS-232 serial cable that had connected the motor to its previous controller whenever it had last been used. The controller is connected to the computer via a homemade RS-232 serial cable with only three of the nine pins connected. The controller receives its power from a 100V wall socket. The gratings in the spectrometer were first successfully turned on

March 27, 2008 using the command line prompt of the MCPI. While finding the
monochromators to be in working order was a success, the overall goal of updating the

```
REAL revs, spd
begin:
INPUT#1, revs, spd

If revs=0 the
goto endp
endif

speed=spd
accel=50
decel=50
movei=revs

waitdone

goto begin

endp:
END
```

Figure 2.5 *MC-BASIC program allowing user-control via serial port*

spectrometer with computer control was to be accomplished using
Labview software which would allow for easy communication
between the computer and the various components of the
spectrometer. The next step was to control the motor using
Labview. This was accomplished by writing an MC-BASIC
program and downloading it into the controller. The program
used is shown in Figure 2.5. This program is downloaded directly
into the controller. When executing the program shown, the
command INPUT#1 causes the program to pause and wait for
input via the serial port. Numbers as hexadecimal strings are sent
via serial port and read into the controller as the variables *revs* and *spd*. Before
movement is executed by the controller, the speed, acceleration, and deceleration
required by the user are set. The desired speed is set from the variable read from the
serial port. The command *movei=[number of revolutions]* executes movement the
desired number of revolutions of the motor. The command *waitdone* tells the controller
to wait until the motor has finished turning before executing any more of the program.
The parts of the program collecting user input and turning the motor are all contained
within a loop that ends once the user enters a value of zero for the number revolutions.
The significance of this program is that it can be run without the MCPI software. Once
the program has been downloaded into the controller, it waits for the */run* command from
the serial port that will begin execution. This enables the user to send the command to

21

run the program as well as the required user input via one of Labview's serial communication modules rather than the MCPI. The program can even be ended in the manner mentioned above without the MCPI. By May 9, 2008, a Labview program had been written with the capability to begin execution of the MC-BASIC program and turn the stepping motor a user-specified number of revolutions. The relationship between the number of motor revolutions and a wavenumber value of the grating position was determined using the analog display of the spectrometer itself, and later versions of the program allowed the user to turn the motor by entering a wavenumber destination and to choose a speed in wavenumbers per second, which would eventually allow for slower or faster scans. By May 15, the motion control program had all the necessary qualities of the one required for Raman spectroscopy. This program allowed the user to control destination and scan speed and was able to keep track of the wavenumber position. It should be noted that there is no electronic output of the spectrometer itself for current wavenumber position. In the past, devices kept up with wavenumber position by being calibrated once and controlling each speed and change in position after that. The Labview program had to keep up with position using a system of timing. The timer has variable input and can adapt to different scanning speeds. The current wavenumber position is calculated constantly during a scan using the starting position, time elapsed since the command to move was executed, and the scan speed. This position is stored in a global variable and displayed on the user interface screen of the program. The position is stored into a text file after the motor has finished turning each time so that the program knows the wavenumber position of the spectrometer even when it has been closed and reopened. This version of the program also contained the option to recalibrate

wavenumber position if the computer's wavenumber position did not match the true position. This happens, for example, if the motor has been turned using the MCPI terminal and the necessary text file not rewritten. A screenshot of the front panel of this program is shown in Figure 2.6. This program looks quite simple, but the graphical code in this version is the same that continues to run the monochromators on the Ramanor.

The next step in the restoration of this Raman spectrometer was to see if the detector and associated equipment were still in working order and to alter the Labview program to collect and record data in addition to control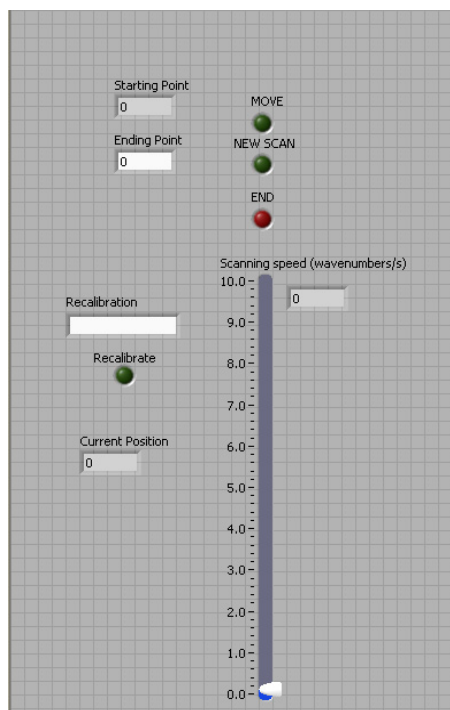ling the diffraction gratings. We received from the University of Tennessee the photomultiplier tube housing and the photomultiplier tube itself. We also received a NIM bin holding many of the electronic components needed to use the photomultiplier tube. The photomultiplier tube housing is cooled by a water bath in addition to being thermoelectrically cooled. The NIM bin included the power source for thermoelectric cooling and the power supply for a no-dew feature for the window of the photomultiplier tube housing. The no-dew feature did not appear to function any longer, but the thermoelectric cooling of the housing was in perfect working order. The photomultiplier tube was outfitted with an IsoTemp circulating bath from Fisher Scientific graciously donated by Dr. Susan Pedigo at the University of Mississippi. The cooled photomultiplier tube is

Figure 2.6 *Labview program with the capability to control the Ramanor's monochromators with user-selected wavenumber positions and display the current wavenumber*

connected to a newly purchased Ortec 556 high voltage power supply at the cathode and an amplifier/discriminator (Ortec 9302) at the anode. The original amplifier/ discriminator in Figure 2.4 was in our possession but appeared to have been replaced by the Ortec model and consequently was not used in the new setup. The output of this amplifier/discriminator is fed to a photon counter (Ortec 770) that was also included in our package of old electronics. Initial tests of the photomultiplier tube connected as mentioned above using brief exposures to room light showed that the photon counter and photomultiplier tube were in working order. The Ortec 770 photon counter has no output that can be read with a computer directly. Research indicated that in the past, scientists using the Ortec 770 counter also used an Ortec 779 interface/controller. At my request, Ortec provided the user's manual for this device, which showed that the interface/controller could be used to read the photon counter data with a computer's serial port.

We were able to buy the interface/controller and test it out in the NIM bin. Using the correct Amphenol fourteen-pin cables, a loop is created between the photon counter and the interface/controller. The interface/controller is capable of resetting the counter to zero and reading the number of counts from it. The interface/controller is connected to a PC via serial cable, and commands are sent from the Labview program similarly as they are to the stepping motor controller. The instruction manual for the interface/controller contained the form of each command that can be read and understood by the device. These commands take the form of four different *control characters*, members of character sets that do not correspond to written symbols. Labview is capable of sending control characters via serial port as their hexadecimal equivalents. The Raman program

was modified then to send through the serial port connected to the interface/controller a "Control T" followed by a "Control R" (hexadecimal 14 and 18 respectively) each time a data point was to be read. These commands cause the interface/controller to read a number of counts from the photon counter and send it to the computer resetting the counter to zero immediately afterward. In the final version of the program, this data collection cycle takes place every 0.02s. The data collection was successfully implemented into the program capable of turning the diffraction gratings, and a few more features were added before the program was finalized. The final version allows selection of different laser lines so that the relative wavenumber data can be read correctly. The final version also includes the option for the user to move the gratings to an absolute or relative wavenumber destination. In addition,
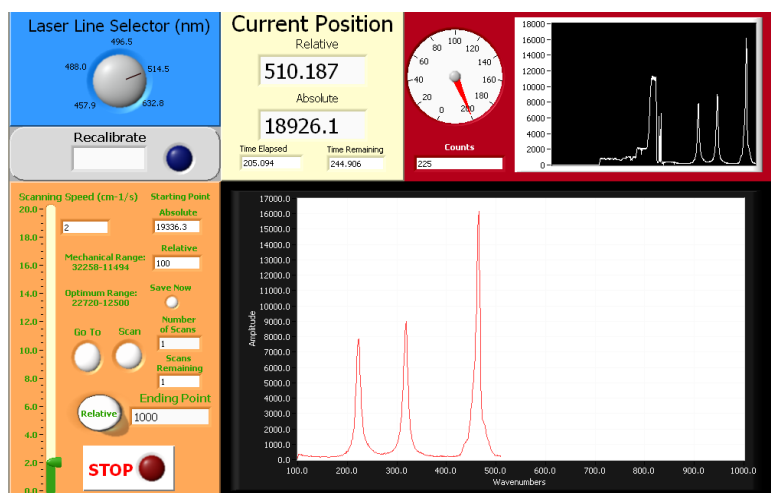
Figure 2.7 *The front panel of the final version of the Labview program controlling the Ramanor and PMT. The spectrum being recorded is of CCl$_4$.*

the final version contains the necessary elements to record multiple spectra and average them. The user selects the number of scans and the spectrometer scans as normal, except it rewinds after each scan to being a new scan. All data is saved to a text file formatted in columns with one column for wavenumber position and one column for each scan. A screenshot of the final version is shown in Figure 2.7. The top right portion reads data from the photon counter every 0.5s and plots it on the chart, displays each value on the

circular gauge, and displays this number in the box labeled *Counts*. To the left of this, wavenumber position in absolute and relative wavenumbers is displayed along with the time elapsed and time remaining for each scan. The top left portion of the screen contains knobs and buttons for laser line selection and recalibration of the computer's wavenumber position with the number displayed on the spectrometer itself. The bottom left portion contains a slider for grating speed selection and number of scans. Here the user selects the destination in units of relative or absolute wavenumbers and whether or not to collect data to save it (*Scan*) or simply move the gratings (*Go To*). Also included here is the option to save spectral data collected even if an entire scan has not been completed. The bottom right portion of the program's front panel is a plot of data collected when a scan is being executed. For a single scan, the chart displays the spectrum as it is being collected. For multiple scans, the chart displays the current scan in addition to the average of all other spectra collected in previous scans.
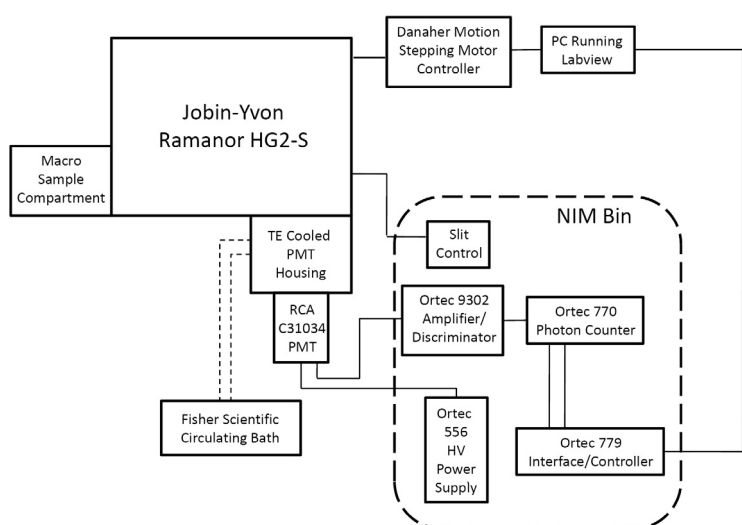
2.3 The New Experimental Setup

Figure 2.8 *Block diagram of the updated Raman spectroscopy setup*

On June 23, 2008, the first spectra were collected using the new experimental setup. A block diagram is shown in Figure 2.8. The first spectra collected were of carbon tetrachloride (CCl_4), one of the original compounds studied by Raman himself and a classic example in any spectroscopy or physical chemistry course. The spectrum is shown in Figure 2.9a. Compare this spectrum to one taken using a CCD camera and microscope as part of the physical chemistry laboratory course at the University of Mississippi (Figure 2.9b). Notice the tremendous difference in resolution. The full-width at half of the maximum of the three leftmost peaks shows how much higher resolution a Raman spectrum can be using the Ramanor instead of more modern instruments and detectors. Also, notice that the spectrum acquired with the Ramanor shows the resolution of both peaks of the Fermi resonance just below 800 cm^{-1}, whereas the Fermi resonance appears as just one broad peak in the second spectrum. The first spectrum also contains several small peaks that probably correspond to other HeNe lines. The high resolution of this first attempt at a spectrum was a victory in perfecting the Raman spectroscopy setup. However, the Ramanor can record spectra with much higher laser power than the 3.0 mW used in the first spectrum, which improves the resolution further. With higher power, the slit width can be closed more and slower scan speeds can be executed, both of which will also increase resolution. Figure 2.9c shows the Raman spectrum of carbon tetrachloride collected around the peak at 459 cm^{-1} in the Figures 2.9a and 2.9b. The spectrum shown is the average of three scans collected with 1 W of laser power with a 1 μm slit width. The mode corresponding to this peak is the totally symmetric stretch wherein all carbon-chlorine bonds lengthen or contract at the same time. Chlorine's most abundant isotopes are ^{35}Cl and ^{37}Cl. These occur in a ratio of

roughly 3:1. This ratio is high enough that modes corresponding to different combinations of chlorine isotopes in CCl_4 can be resolved in the Raman spectrum. Since one out of every four chlorine atoms should be the less naturally occurring isotope, the most intense peak in the spectrum corresponds to CCl_4 with one ^{37}Cl and three ^{35}Cl atoms. Just as masses oscillating on a spring have a frequency of vibration inversely proportional to their reduced mass, the frequency of the totally symmetric stretch will increase as the reduced mass is decreased. As a result, we know that the peak at higher frequency than the most intense peak is due to CCl_4 with four ^{35}Cl atoms. The other two peaks shown correspond to CCl_4 di-substituted and tri-substituted with ^{37}Cl atoms. The peak corresponding to CCl_4 with four ^{37}Cl atoms could not be resolved. The rarity of this combination means the peak produced is too weak to detect.
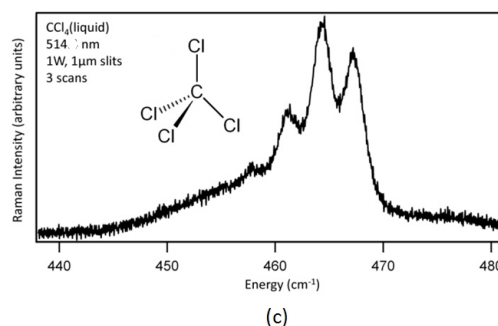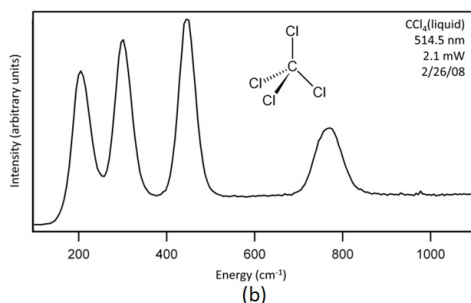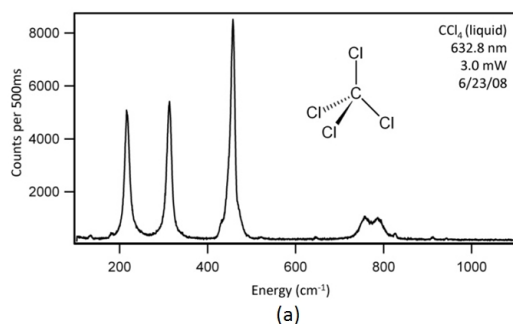

Figure 2.9 a) *First Raman spectrum acquired with the new and improved experimental setup.* **b)** *Raman spectrum acquired using CCD camera and microscope.* **c)** *Raman spectrum showing resolved isotopic peaks.*

The last major obstacle in putting a Raman spectroscopy experimental setup into place came shortly after the first spectrum was collected in switching from a HeNe laser to an Ar^+ laser. An Ar^+ laser emits light that is polarized while a HeNe laser's light is

generally not. As noted in the first section of this manuscript, Raman scattered light is polarized. This effect is most noticeable when the source illumination is polarized. Imagine a totally symmetric mode as described above. The polarizability change during this vibration changes the same way in all directions. The electric field of plane polarized light then will induce a dipole moment in a direction parallel to the electric field. Most of the Raman scattered light will be polarized in the same direction as the incident light and scattered at all angles perpendicular to this polarization. Collecting light perpendicularly to the laser as with the Ramanor requires vertically polarized light. Otherwise, totally symmetric modes appear with much lower intensity. Other modes may also be affected, but since their interaction with the electric field is more complicated, they may not always exhibit peaks at a greatly reduced intensity. Our setup used horizontally polarized Ar^+ laser light. In switching from the HeNe to the Ar^+ laser, the intensity of the totally symmetric mode of benzene at 990 cm^{-1} was being monitored for signal optimization purposes and was found to be drastically reduced in intensity with the new laser despite higher power. From this, it was determined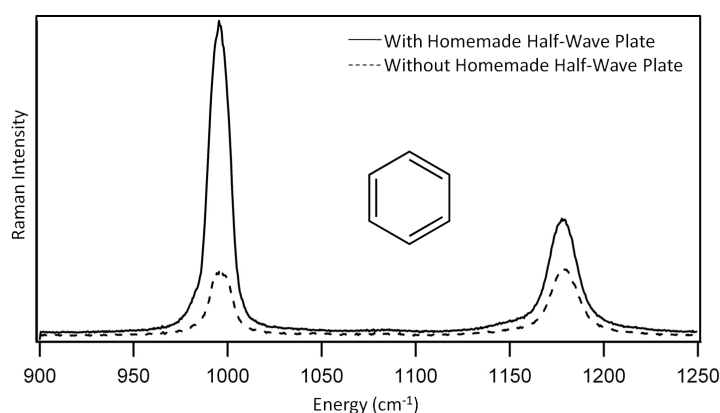 that the laser light was polarized incorrectly for our setup. The plane of polarization of light can be rotated ninety degrees by means of a half-wave plate. We constructed our own half-wave plate using a microscope slide and glossy cellophane tape as suggested in an optics textbook.[2] The results are

Figure 2.10 *The effect of a half-wave plate on two benzene peaks. The half-wave plate rotates the plane of polarization of the laser ninety degrees.*

29

shown in Figure 2.10. The totally symmetric mode at 990 cm^{-1} decreases greatly in intensity when the laser polarization is not rotated to be vertical. Notice the mode at higher energy is not changed as much because it is not totally symmetric. A commercial grade half-wave plate was purchased for use in the final version of the experimental setup.

2.4 References

(1)   Armstrong, D. P.; Fletcher, W. H.; Trimble, D. S. *Data Acquisition and Control of a Raman Spectrometer Using A DEC PDP 11/34 Computer*, Oak Ridge Gaseous Diffusion Plant, 1987.

(2)   Hecht, E. *Optics*; Second ed.; Addison, 1987.

3 Raman Spectroscopic Investigations of Intermolecular Interactions Involving Pyrimidine

Presented here is an investigation of intermolecular interactions involving pyrimidine (1,3-Diazabenzene) using Raman spectroscopy. Room temperature Raman vibrational spectra of pyrimidine were obtained at atmospheric pressure and at elevated pressures up to 30000 psi to probe the effects of weak hydrogen bonds in crystalline pyrimidine. Additionally, Raman spectra of binary mixtures of pyrimidine and varying concentrations of seven other molecules were acquired to investigate strong hydrogen bonds in terms of the evolution of the Raman spectrum with changing compositions of the mixtures.
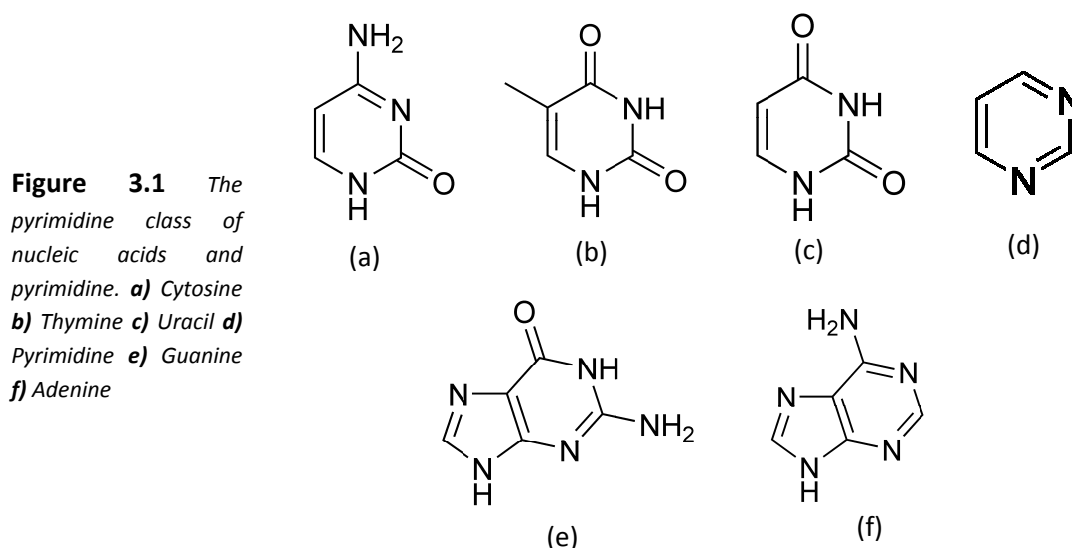
3.1 Introduction

Hydrogen bonding, a weak intermolecular interaction, is an extensively investigated phenomenon due to its importance in the chemical and physical properties of water, the compound most essential to life on earth, as well as its importance in the structure and function of biomolecules including amino acids, nucleotides, monosaccharides, and the polymers formed from these molecules.[1] Hydrogen bonding has been

investigated since the 19th century, even before the term *hydrogen bond* was coined by Linus Pauling in a 1931 paper on the nature of the chemical bond.[2,3] Typically, hydrogen bonding occurs between an electron deficient hydrogen atom (covalently bonded to an electronegative atom) and another electronegative element with lone electron pairs.[1] Another weak intermolecular interaction important in biological systems is the so-called π stacking interactions between the delocalized π systems of aromatic molecules.[4] Nitrogen-containing aromatic heterocycles are suitable prototype molecules for studying these interactions, as they have the ability to participate in both hydrogen bonding through the nitrogen atom and π stacking through the delocalized π system. Vibrational spectroscopy, both infrared (IR) and Raman, lends itself to studies of these interactions.[5] Changes in a vibrational spectrum allow us to ascertain exactly which atoms and bonds are being affected in the intermolecular interactions taking place and to what extent these interactions are occurring. Hydrogen bonds have been investigated with Raman spectroscopy as far back as the 1950s when Puranik investigated hydrogen bonds between donors and carbonyl acceptors[6-8] and found the first evidence in a Raman spectrum for hydrogen bonds to nitrogen.[9] Vibrational spectroscopy has also been used to investigate hydrogen bonding in terms of thermodynamic properties including association constants,[10] rate constants,[11] and formation enthalpies.[12]

In this study, we investigate the Raman spectrum of pyrimidine under different conditions. Pyrimidine, from which the nucleobases known as *pyrimidines* are derived, is shown in Figure 3.1 along with the pyrimidine nucleobases cytosine, thymine, and uracil. Also shown in Figure 3.1 are the remaining nucleobases prevalent in nucleic acids, known as the purines. Notice that these molecules also contain six-membered

rings consisting of two nitrogen atoms. It should be apparent then that pyrimidine can participate in similar non-covalent interactions as the purines and pyrimidines present in nucleic acids. Futhermore, three of the twenty essential amino acids (tryptophan, tyrosine, and phenylalanine) contain aromatic groups. The study of non-covalent interactions of pyrimidine could then lead to a better understanding of intermolecular interactions occurring in DNA, RNA, and proteins all of which contain molecules with structural and chemical similarities to pyrimidine.

Figure 3.1 *The pyrimidine class of nucleic acids and pyrimidine. **a)** Cytosine **b)** Thymine **c)** Uracil **d)** Pyrimidine **e)** Guanine **f)** Adenine*

Pyrimidine and other nitrogen containing heterocycles are well-studied molecules, with the first Raman spectrum of pyrimidine being published in 1957.[13] In this study, we investigate specifically spectral shifts of the ν_1 peak corresponding to the ring-breathing mode, in which all bonds of the ring lengthen or contract simultaneously. In 1963, Fratiello found that the ring-breathing peak in the Raman spectrum of pyridine shifted to higher frequencies with higher concentrations of water.[14] In 1966, Takahashi carried out a thorough investigation of the IR spectra of the azabenzenes pyridine, pyrimidine,

pyrazine, and pyridazine in various hydrogen bond donor and non-donor solvents.[15] Takahashi also found the v_1 peaks of the various azabenzenes investigated to shift to higher frequency upon hydrogen bond formation. Takahashi mentions briefly the possibility that the blue-shift must be due to a considerable shift in electron density, citing a comparison of his spectra to the vibrational spectrum of the pyridinium cation published by Cook.[16] More recently, hydrogen bonding in pyridine mixtures has been investigated by monitoring the shift of the v_1 peak in mixtures of ethanol[17] and water[18,19] and in terms of the shift of water's peaks in a vibrational spectrum.[20] Pyrimidine was most recently investigated in 2007 when Schlucker and coworkers investigated theoretically and experimentally the shift of the v_1 peak of the Raman spectrum in mixtures of varying amounts of water.[5] Their calculations showed that the wavenumber shift, which should be indicative of the degree of hydrogen bonding taking place, showed a "perfect negative correlation" with the bond distance between nitrogen and the hydrogen on water molecules and the wavenumber position of v_1. This correlation, however, only exists within certain subgroups of pyrimidine and water clusters. Within these subgroups, increasing water concentration leads to increased wavenumber position of v_1. The "water concentration" in their calculations was increased by adding more water molecules in positions to hydrogen bond with pyrimidine or with water molecules already present. The subgroups in which the negative correlation holds are those in which water molecules are added that hydrogen bond to other water molecules and not to pyrimidine. Their conclusions seem to indicate the large role of a hydrogen bonded network versus single hydrogen bonds to pyrimidine in wavenumber position of the ring-breathing mode of pyrimidine. In our study, we wished to investigate further the

hydrogen bonding in pyrimidine. We monitored the position of ν_1 in the Raman spectrum of pyrimidine in mixtures of pyrimidine and various concentrations of water, methanol, benzyl alcohol, 1-hexanol, acetic acid, hexylamine ($CH_3(CH_2)_5NH_2$), acetonitrile (CH_3CN), ethylene glycol ($HOCH_2CH_2OH$), and 2-mercaptoethanol ($HOCH_2CH_2SH$). In addition, we monitored the position of other vibrational modes, and we acquired Raman spectra of pyrimidine under high pressure to investigate the weak hydrogen bonding in neat pyrimidine as the liquid crystallizes. Below, we also clear up a few discrepancies present in the literature regarding the symmetry of certain normal modes.

3.2 Experimental

Commercially obtained pyrimidine (Sigma Aldrich) was used in all experiments without further purification. All Raman spectra were recorded using a Jobin-Yvon HG2-S Raman spectrometer with a double grating monochromator and photomultiplier tube detector as described in Chapter 2 of this manuscript. Data were collected using a custom Labview program written for control of the spectrometer and data collection. The exciting source used throughout the experiment was the 514nm line of a Coherent Innova 200 Ar^+ laser with 1W of power. A laser line filter was used to ensure the sample was only being excited with 514nm line. A half-wave plate (Thor Labs) was used to rotate the laser polarization so that the sample was illuminated with vertically polarized light. Mixtures were prepared using Fisher finnipipettes. Pressure studies were carried out using a custom pressure cell with quartz windows attached to a 10 cm^3 piston press (High Pressure Equipment Company). Pyrimidine was placed in a glass bottle capped with a

small section of polyethylene tubing sealed at one end. The piston and cell were filled with ethanol, and the bottle was placed in the proper position inside the cell. The entire system was sealed, and the press was used to change the height of the piston and thereby the pressure inside the system. Pressure was monitored by means of a gauge attached to the piston. Geometry optimizations and frequency calculations were performed using the Gaussian 03 software package[21]. All calculations used the B3LYP hybrid functional with a 6-311G(d,p) basis set.

3.3 Results and Discussion

Weak Hydrogen Bond in Crystalline Pyrimidine

Shown in Figure 3.2 is the Raman spectrum of liquid pyrimidine at 20°C. An exhaustive literature search showed that only one other Raman spectrum of pyrimidine ever published shows the same level of detail, i.e. resolution of peaks and presence of
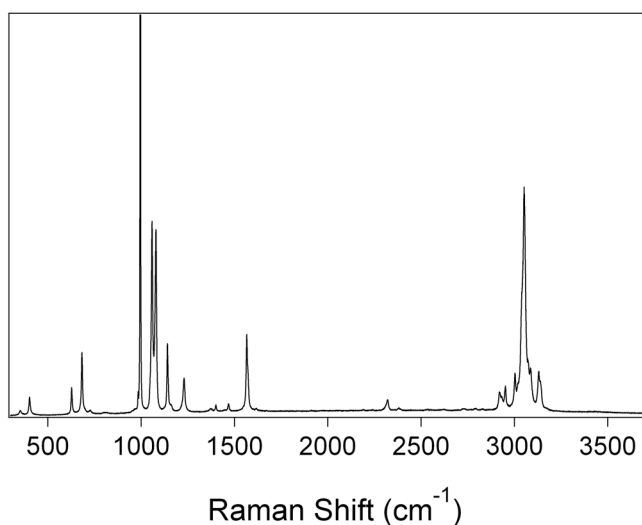
Figure 3.2 *Raman spectrum of neat pyrimidine.*

combination bands[22]. The most intense peak in the spectrum corresponds to ν_1. To ensure local heating effects were not influencing spectra because of the high laser power,

spectra of pyrimidine were collected at lower power and showed no difference in the position or relative intensity of peaks. The high power was used merely to achieve the highest signal-to-noise ratio in the Raman spectrum. Shown in Figure 3.3 are the Raman spectra of pyrimidine at pressures 10000 psi, 20000 psi, and 30000 psi in addition to the spectrum at atmospheric pressure (14.7 psi) all of which were acquired in the high pressure cell filled with ethanol. Regions of interest are shown in greater detail and discussed below. From comparison of the spectra at 30000 psi and solid pyrimidine
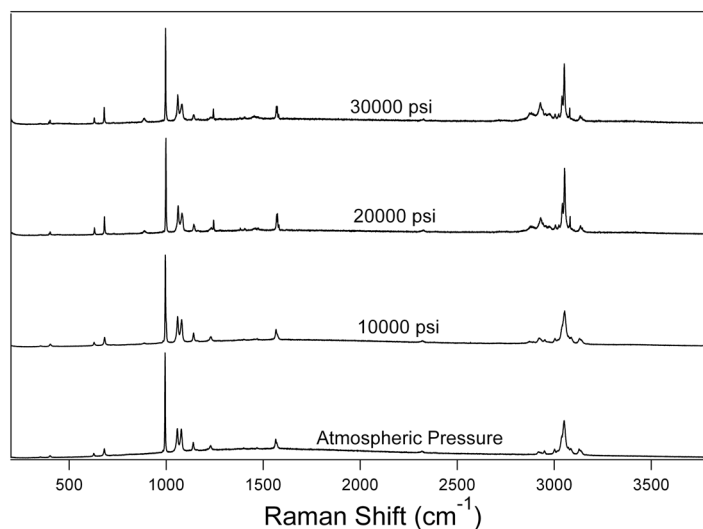
Figure 3.3 *Raman spectra of pyrimidine at elevated pressures. Pyrimidine crystallizes between 20000 psi and 30000 psi.*

(3°C, atmospheric pressure), it was determined that pyrimidine crystallizes at some pressure between 20000 psi and 30000 psi. The conclusion is that intermolecular interactions of the liquid molecules are maximized somewhere between these two pressures just before the solid is formed. Figure 3.4 shows the 400-800 cm^{-1} region of Figure 3.3 enlarged. Notice the peak at 352 cm^{-1} reduces in intensity and disappears into the baseline as pyrimidine is crystallized. This peak corresponds to an out of plane

bending of the atoms of the ring. The peak at 401 cm^{-1} splits into two peaks as pyrimidine crystallizes. This peak corresponds to another out of plane bending of the atoms of the ring. These two modes are pictured in Figure 3.5. The changes in these peaks reflect the changes in pyrimidine as it crystallizes. The mode at 352 cm^{-1} must
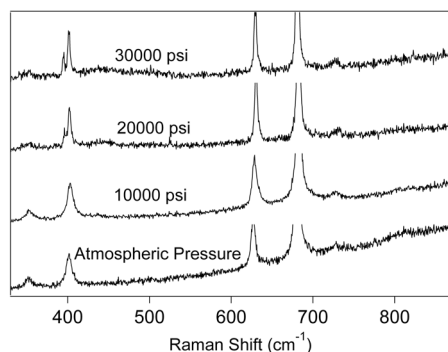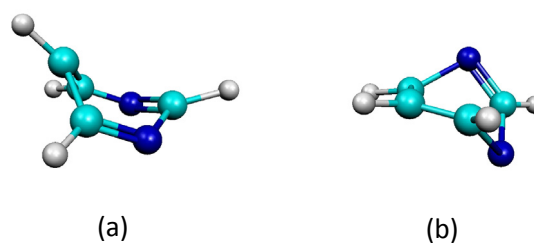

Figure 3.4 *Enlarged version of Figure 3.3*

(a)   (b)

Figure 3.5 *Two normal modes of pyrimidine at their maximum amplitudes corresponding to Raman peaks at **a)** 352 cm^{-1} and **b)** 402 cm^{-1}*

cease to occur or only occur less as pyrimidine crystallizes. Furthermore, the mode at 401 cm^{-1} must split into two peaks because of two different environments in which the mode occurs. That is, in the crystal structure of pyrimidine, a fraction of the pyrimidine molecules must exist in an environment where the vibration pictured in Figure 3.5b cannot occur as it does elsewhere in the crystal. The unit cell of the actual crystal structure of pyrimidine is pictured in Figure 3.6.[23] The intermolecular interactions

Figure 3.6 *Unit cell of the crystal structure of pyrimidine. Dotted lines indicate intermolecular interactions or weak hydrogen bonds.*
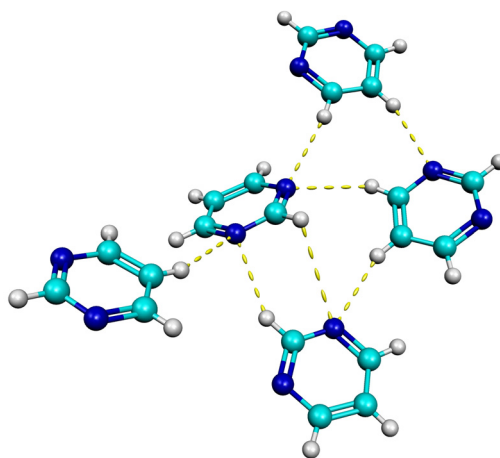
occurring in the crystal structure are indicated by the broken lines. Note that these are not the strong hydrogen bonds between electronegative elements and hydrogen atoms bonded other electronegative elements. These are weak interactions forced when pressure is increased or when the temperature is decreased causing crystallization. The location of these interactions shows clearly how the modes pictured in Figure 3.5 are perturbed as pressure is increased. An enlargement of the 2900-3200 cm^{-1} region of Figure 3.3 is shown in Figure 3.7. Here, we see similar changes occurring, but in the CH stretching region of the spectrum. Note the appearance
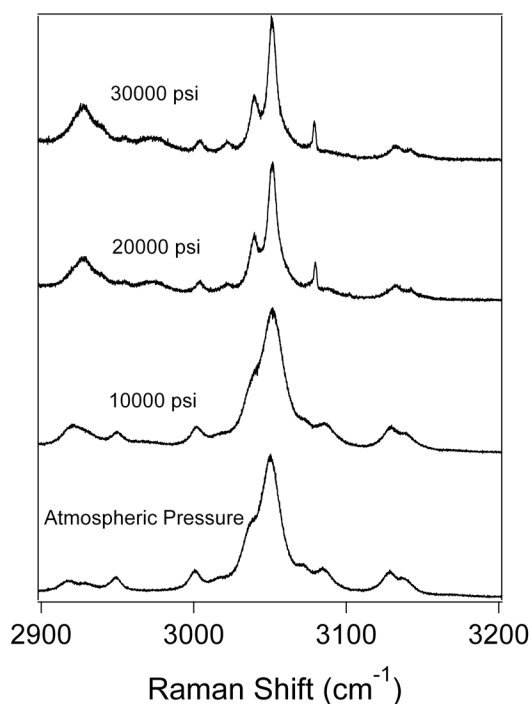

Figure 3.7 *Raman spectra of pyrimidine at the indicated pressures. Note the change in the mode at 3079cm^{-1} discussed in the text.*

of the peak at 3079 cm^{-1}. This peak is present at all pressures but becomes much sharper and more pronounced as the pressure is increased. This peak corresponds to the CH stretch for the CH group not connected to any nitrogen atoms. Note in the crystal

structure that the shortest intermolecular distance is between the hydrogen atom in this CH group and a nitrogen atom on a neighboring pyrimidine molecule. The crystal structure would lead us to believe that this is a relatively strong interaction, and the Raman spectrum indicates that this is indeed the case. Similar changes can be seen elsewhere in the CH stretching region of the spectrum, but that discussed above can be seen to be the most pronounced, presumably because this interaction is forced to occur strongly as pyrimidine is crystallized.

Strong Hydrogen Bonds in Pyrimidine Binary Mixtures

Water

Our first step in this study was to repeat the experiment by Schlucker[5] and compare the results. We prepared mixtures of pyrimidine with varying mole fractions of water and collected the Raman spectrum of each. The results are shown in Figure 3.8. We were
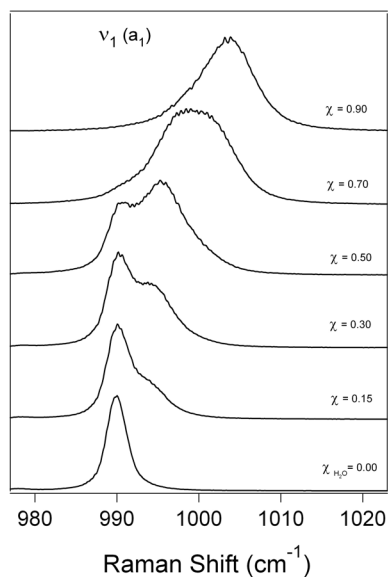

Figure 3.8 *Raman spectra of mixtures of pyrimidine with the indicated mole fractions of water monitoring the position of v_1*

able to replicate the previous results. The peak v_1 was found to shift by 13cm^{-1} (from 990 cm^{-1} to 1003 cm^{-1}) as the amount of water present was increased. It is important to note that the peak continues to increase while more water is added. Our group also found

40

other shifts in the Raman spectrum of pyrimidine to occur. Shown in Figure 3.9 are four other regions of the spectrum where similar albeit smaller blue shifts of pyrimidine peaks occur as more water is added. Vibrations corresponding to ν_{16a} and ν_{16b} were discussed above and shown in Figure 3.5. ν_{6a} and ν_{6b} correspond to in-plane ring modes. ν_{9a}, ν_{15}, and ν_3 are due to in-plane CH wagging modes. There has been discrepancy in the literature in the past over the proper assignment and symmetry of the peaks shown in the bottom two spectra of Figure 3.9 (Refs. 13, 15, 17, and 22, e.g.). To make definitive assignments, Figure 3.10 shows polarized Raman spectra collected showing the modes
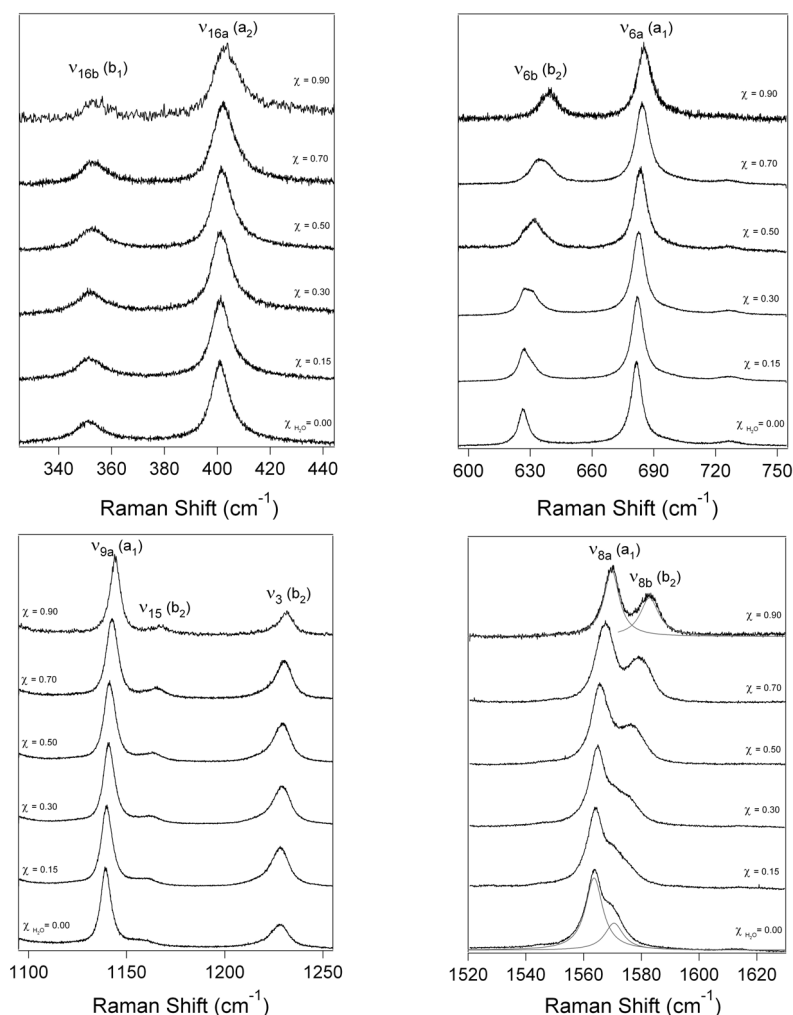

Figure 3.9 *Other blue shifting peaks in the Raman spectrum of pyrimidine. ν_{8a} and ν_{8b} were fitted to Gaussian curves to clearly show their positions even when the two could be not be fully resolved. Each mode is described in the text.*

in question. The drastic reduction in intensity of the peaks we have assigned to ν_{8a} and ν_{9a} shows that they do possess a_1 symmetry and thus have been assigned correctly. Interestingly, Figure 3.10 indicates that peaks corresponding to ν_{8b} and ν_{15} shift noticeably while the neighboring peaks shift very little, if at all.
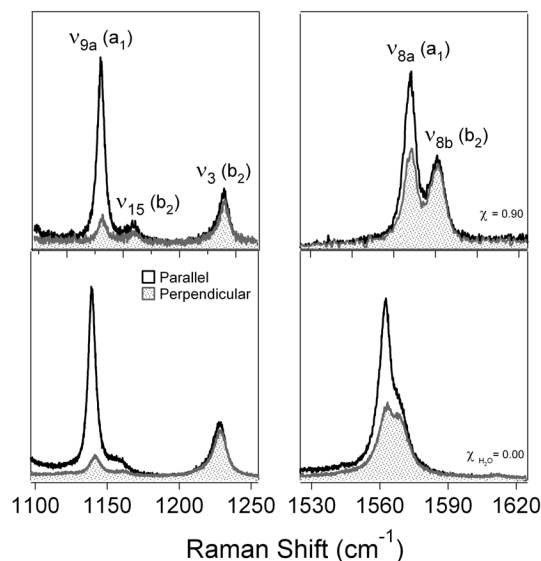

Figure 3.10 *Polarized Raman spectra. Parallel* refers to the fact that polarizer film *was employed to collect only Raman scattered light that was polarized parallel to the laser polarization.* Perpendicular *refers to spectra collected by rotating the same polarizer film ninety degrees. A drastic reduction in intensity indicates a peak corresponding to a mode of a_1 symmetry.*

According to Schlucker's calculations, the hydrogen bond strength present in the pyrimidine-water system is found to increase predictably only for new water molecules hydrogen bonding to water (already hydrogen bonded with pyrimidine). Optimized structures for several configurations of water hydrogen bonding with pyrimidine are shown in Figure 3.11. Notice the network of hydrogen bonds that results when more water molecules are included as opposed to hydrogen bonds occurring only between water molecules and pyrimidine.

Methanol

To investigate whether or not this continuous shift of the v_1 peak was indeed due to the hydrogen bond network formed by water molecules, we performed the same experiment with methanol as the hydrogen bond donor. Although there are a myriad of possibilities for combinations of water molecules hydrogen-bonding with each other and with pyrimidine, there are only two combinations possible with a molecule such as methanol because it lacks the ability to form a network as water does. The two possible combinations are shown in Figure 3.12. Raman spectra for the methanol experiment are shown in Figure 3.13.
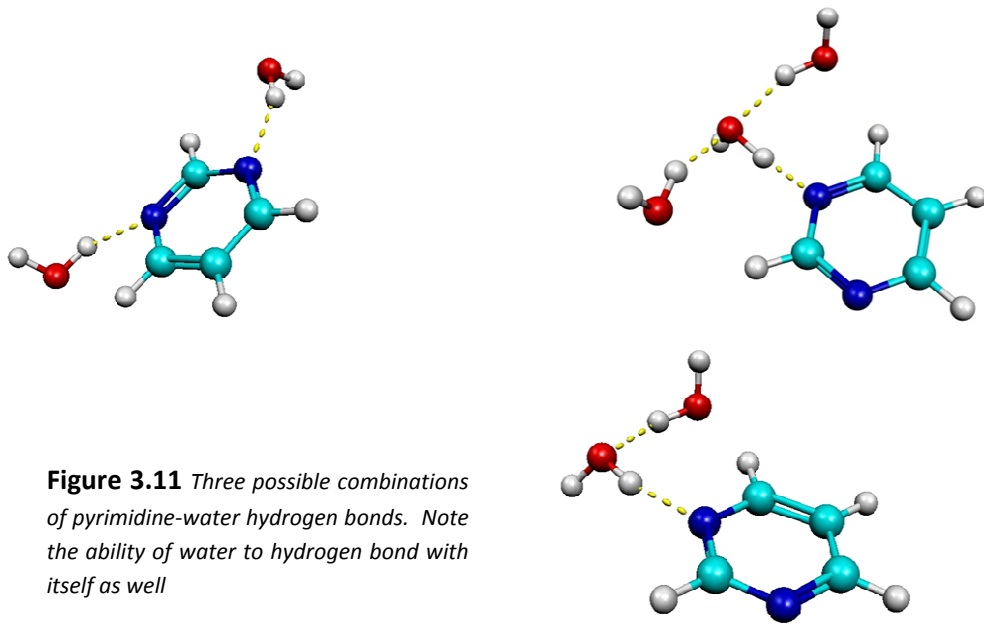

Figure 3.11 *Three possible combinations of pyrimidine-water hydrogen bonds. Note the ability of water to hydrogen bond with itself as well*
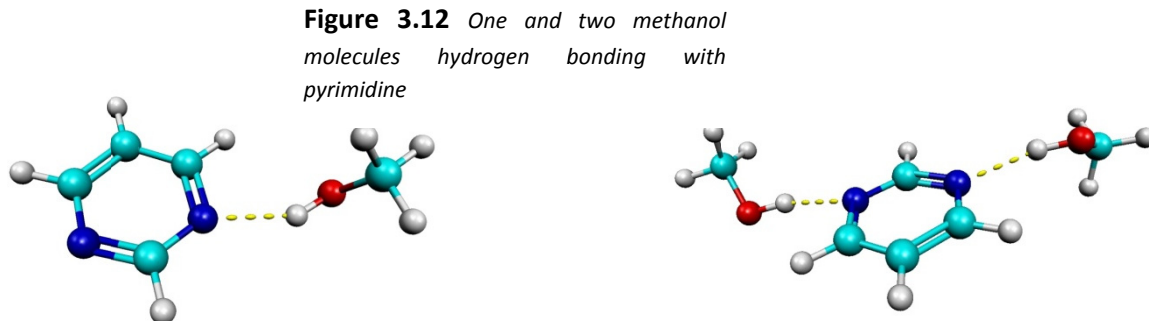
Figure 3.12 *One and two methanol molecules hydrogen bonding with pyrimidine*
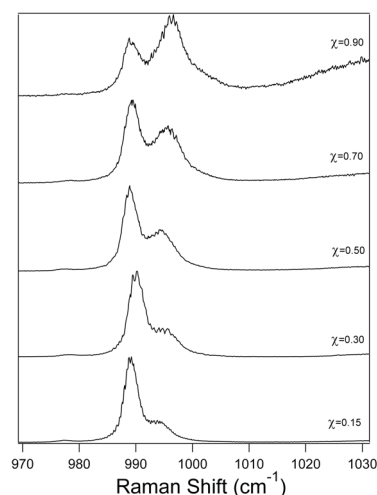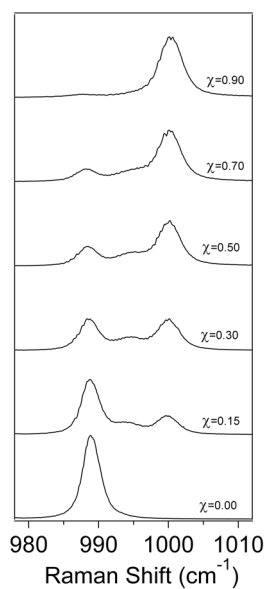
Figure 3.13 *Raman spectra of mixtures of pyrimidine with the indicated mole fractions of methanol monitoring the position of v_1. The broad peak at $1030cm^{-1}$ in the spectrum corresponding to a mole fraction of 0.90 methanol is due to methanol itself.*

Figure 3.13 shows that v_1 is blue-shifted when the hydrogen bond donor is methanol just as when the hydrogen bond donor is water. The shift of 9 cm^{-1} is, however, less than the shift seen with water. Furthermore, the shift is very little after the first aliquot of methanol is added. This indicates that whatever species is responsible for the shifted peak is present as soon as any methanol is added. This differs from water in that addition of water caused continuously further shifting, indicating that new hydrogen bonded species were being formed as more water was added. Frequency calculations were performed on both hydrogen-bonded species of pyrimidine and methanol and the pyrimidine monomer. Frequencies were scaled such that the v_1 peak of the monomer matched the experimental spectrum. The calculated (and scaled) frequency for v_1 for the pyrimidine hydrogen-bonded with one methanol system was 994 cm^{-1}. This calculated frequency matches exactly the shifted peak seen in the spectrum of 50% mole fraction. This is reasonable because there should be one methanol molecule for each pyrimidine molecule in this mixture, meaning the shifted peak should be due to the species for which the calculation was performed. Frequencies were also calculated and scaled for the system of pyrimidine hydrogen bonded to two methanol molecules. The calculated v_1

frequency of this system was 1001 cm^{-1}. The experimentally observed shifted peak only

shifts to a frequency of 997 cm^{-1} for a mole fraction of 90% methanol. We can conclude

from these data that even with a 9:1 ratio of methanol molecules to pyrimidine molecules,

the doubly hydrogen bonded pyrimidine is not the prevalent species. ν_1 still shifts,

however, with mole fractions of water greater than 0.50. The average number of

methanol molecules hydrogen bonded to one pyrimidine molecule must between one and

two.

Benzyl Alcohol, 1-Hexanol, and Hexylamine

To investigate further the shifting of the ν_1 peak or pyrimidine with hydrogen bonding

and the cause of the continuous shifting, benzyl alcohol, 1-hexanol, and hexylamine were

also investigated similarly to methanol and water above. These molecules are only

capable of forming hydrogen bonds at one location. Therefore, their spectra were

expected to exhibit similar properties as the spectrum of methanol. The spectra are

shown in Figure 3.14. The spectra of mixtures of pyrimidine and alcohols exhibit similar

behavior to the spectra of methanol above. In Figure 3.17a, the blue-shifted peak can be

found between the ring-breathing peak ν_1 of pyrimidine at 990 cm^{-1} and the ring-

breathing peak of benzyl alcohol at 1000 cm^{-1}. As with methanol, the blue-shifted peak

has an immediate appearance with the 15% mole fraction mixture, and the shift in

subsequent mixtures is very little. Again, the peak does not shift as much as the peak due

to hydrogen bonds with water. The spectrum of 1-hexanol in Figure 3.14b shows similar

behavior to the methanol spectra also. The spectra of mixtures of hexylamine do not

exhibit the same behavior as the alcohols, however. Figure 3.14c shows that the position
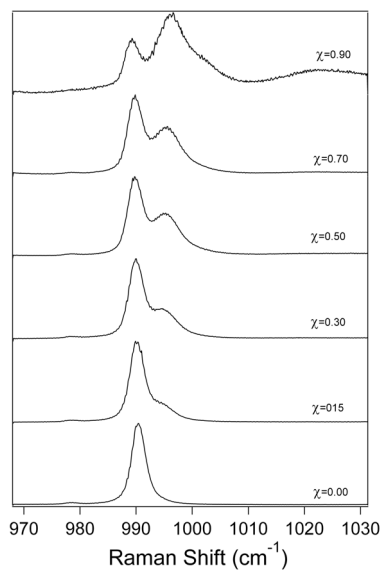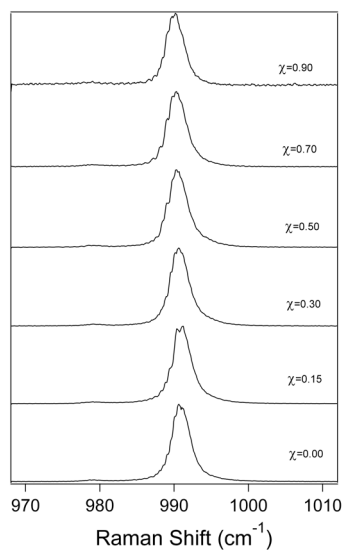
Figure 3.14 *Raman spectra of mixtures of pyrimidine and varying mole fractions of **a)** benzyl alcohol, **b)** 1-hexanol, and **c)** hexylamine*

of ν_1 does not change appreciably with any amount of hexylamine added. We would expect that hexylamine participates in hydrogen bonding with pyrimidine. However, due to the lower electronegativity of nitrogen compared to oxygen, the hydrogen bonds formed may be weaker and therefore unable to cause a measurable shift.

Acetic Acid and Ethylene Glycol

We continued the investigation with hydrogen bond donors that have the ability to hydrogen bond with pyrimidine and with each other. These molecules would be expected to exhibit hydrogen bonding properties resembling water more than the alcohols investigated above. The data are shown in Figure 3.15.
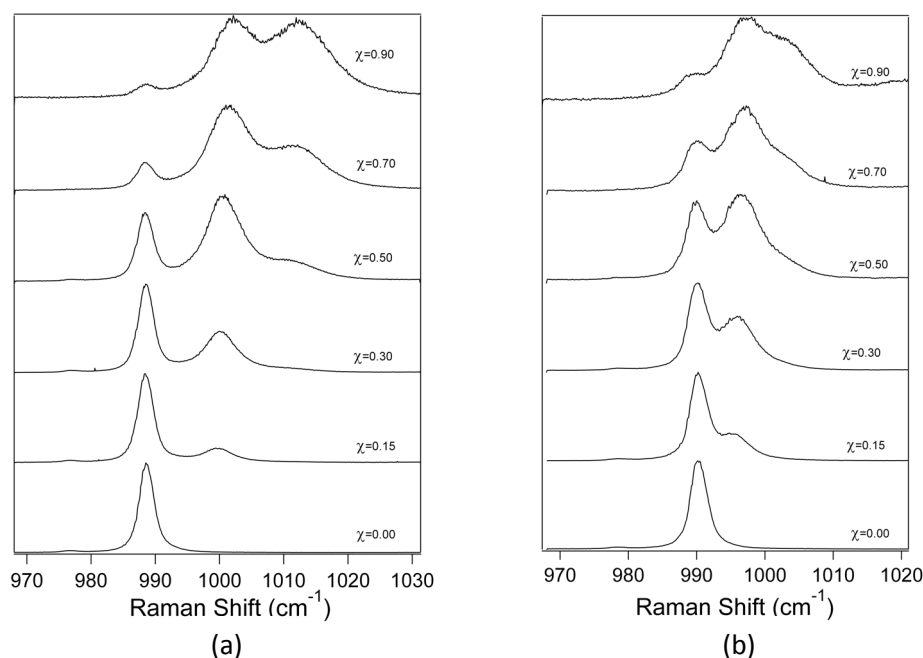

Figure 3.15 *Raman spectra for mixtures of pyrimidine and varying mole fractions of **a)** acetic acid and **b)** ethylene glycol*

Figure 3.15a shows the Raman spectrum for mixtures of pyrimidine and acetic acid. The highest energy peak high mole fraction of acetic acid mixtures is due to acetic acid. The peak between ν_1 and this peak due to acetic acid is the blue-shifted peak of interest. The shift of this peak to 13 cm^{-1} higher energy shows that the strength of this hydrogen bond is probably more comparable that of pyrimidine with water. However, the gradual and continuous shift seen with water is not seen with acetic acid. This

indicates that despite the fact that acetic acid can form hydrogen bonds with itself (and thus forms the network that seems important in the position of ν_1 pyrimidine-water hydrogen bonds), this network does not seem to have the same effect when it is formed by acetic acid. The spectra of mixtures of ethylene glycol and pyrimidine shown in Figure 3.15b contain some interesting features as well. Mixtures up to the 50% mole fraction of ethylene glycol show a blue-shifting of ν_1 as expected. Comparison with Figure 3.15a shows this shift is not as a great as for acetic acid. The 70% and 90% mole fraction mixtures show something not seen in other systems studied thus far. There is the clear appearance of a third peak shifted a full 13 cm^{-1} from the original pyrimidine peak. At high concentrations of ethylene glycol, there must exist three distinct species of ethylene glycol hydrogen-bonding with pyrimidine. These species could be any of a number of configurations of ethylene glycol and pyrimidine since ethylene glycol has two sites capable of hydrogen bonding. What is interesting is that this third new species only appears to be present in appreciable concentrations when the ethylene glycol makes up a 90% mole fraction of the entire mixture.

Acetonitrile

Our final investigation was to repeat the experiment yet again with acetonitrile as the molecule mixed with pyrimidine. Acetonitrile is not capable of donating hydrogen atoms for hydrogen bonding. It would not be expected therefore to cause the shift attributed to hydrogen bonding in the above cases. However, we wished to make sure that the effect seen was not one due to polarity of the solvent. Since acetonitrile is highly polar while not being able to hydrogen bond, this molecule was ideal for this purpose. The results are shown in Figure 3.17. As we can see, ν_1 does not shift at all with addition of acetonitrile.

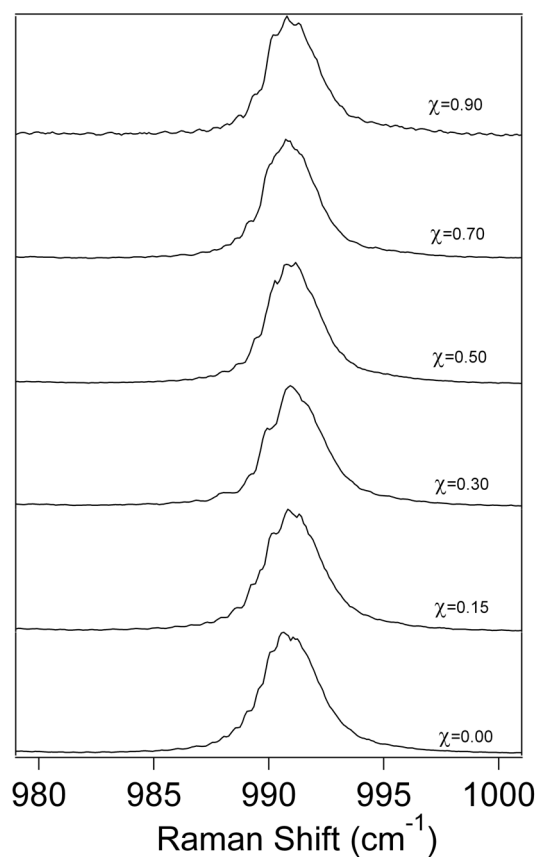These results show that the shifts are due to hydrogen bonding and not due to a solvent polarity effect.

Figure 3.17 *Raman spectrum of pyrimidine and varying mole fractions of acetonitrile*

3.4 Conclusion

Hydrogen bonding between pyrimidine and various donors and acceptors was investigated using Raman spectroscopy to measure the positions of bands in the spectra. Previous studies have shown the band ν_1 to be a suitable marker for the degree of hydrogen bonding in pyrimidine.[5] We found that other bands shift as well in mixtures of pyrimidine and water. We also found different behaviors of the shifts of pyrimidine in mixtures of hydrogen donors other than water. Methanol was found to cause a shift that

49

was smaller in magnitude and less continuous than the shift caused by water. Our calculations showed this to be due to the formation of pyrimidine molecules hydrogen bonding with an average of between one and two methanol molecules. This difference in shift may also be due to the inability of methanol to hydrogen bond with itself and with pyrimidine. Benzyl alcohol and 1-hexanol were found to exhibit similar effects. Hexylamine was found to cause no shift in pyrimidine's peak, presumably because the hydrogen bonds exhibited are weaker. Acetic acid and ethylene glycol showed effects similar in magnitude with water. Acetic acid, however, did not cause the gradual shift caused by water. Furthermore, ethylene glycol caused the appearance of a third peak at very high concentrations.

3.5 References

(1)   Hobza, P.; Havlas, Z. *Chemical Reviews* **2000**, 4253-4264.

(2)   Jeffrey, G. A. *An Introduction to Hydrogen Bonding*; Oxford University Press: New York, **1997**.

(3)   Pauling, L. *Journal of the American Chemical Society* **1931**, *53*, 1367-1400.

(4)   Bates, D. M.; Anderson, J. A.; Oloyede, P.; Tschumper, G. S. *Physical Chemistry Chemical Physics* **2008**, *10*, 2775-2779.

(5)   Schlucker, S.; Koster, J.; Singh, R. K.; Asthana, B. P. *Journal of Physical Chemistry A* **2007**, *111*, 5185-5191.

(6)   Puranik, P. G. *Proceedings-Indian Academy of Sciences, Section A* **1953**, *37A*, 499-503.

(7)   Puranik, P. G. *Proceedings-Indian Academy of Sciences, Section A* **1953**, *38A*, 233-238.

(8)   Puranik, P. G. *Journal of Chemical Physics* **1957**, *26*, 601-603.

(9)   Puranik, P. G. *Proceedings-Indian Academy of Sciences, Section A* **1957**, *45A*, 51-57.

(10)   Kasende, O.; Zeegers-Huyskens, T. *Spectroscopy Letters* **1980**, *13*, 493-502.

(11)   Cabaco, M. I.; Besnard, M. *Molecular Physics* **1992**, *75*, 157-172.

(12)   Kim, J. H.; Lee, H.-J.; Eun-Jung Kim; Jung, H. J.; Choi, Y.-S.; Park, J.; Yoon, C.-J. *Journal of Physical Chemistry A* **2004**, *108*, 921-927.

(13)   Lord, R. C.; Marston, A. L.; Miller, F. A. *Spectrochimica Acta* **1957**, *9*, 113-125.

(14)   Fratiello, A. *Journal of the American Chemical Society* **1963**, *85*, 3072-3075.

(15)   Takahashi, H.; Mamola, K.; Plyler, E. K. *Journal of Molecular Spectroscopy* **1966**, *21*, 217-230.

(16)   Cook, D. *Canadian Journal of Chemistry* **1961**, *38*, 2009-2024.

(17)   Deckert, V.; Asthana, B. P.; Mishra, P. C.; Kiefer, W. *Journal of Raman Specroscopy* **1996**, *27*, 907-913.

(18)   Schlucker, S.; Singh, R. K.; Asthana, B. P.; Popp, J.; Kiefer, W. *Journal of Physical Chemistry B* **2001**, *105*, 25A-25A.

(19)   Schlucker, S.; Heid, M.; Singh, R. K.; Asthana, B. P.; Popp, J.; Kiefer, W. *Zeitschrift Fur Physikalische Chemie-International Journal of Research in Physical Chemistry & Chemical Physics* **2002**, *216*, 267-278.

(20)   Maes, G.; Smets, J.; Adamowicz, L.; McCarthy, W.; VanBael, M. K.; Houben, L.; Schoone, K.; Elsevier Science Bv: 1997, p 315-322.

(21)   M. J. Frisch, G. W. T., H. B. Schlegel, G. E. Scuseria, ; M. A. Robb, J. R. C., J. A. Montgomery, Jr., T. Vreven, ; K. N. Kudin, J. C. B., J. M. Millam, S. S. Iyengar,

J. Tomasi, ; V. Barone, B. M., M. Cossi, G. Scalmani, N. Rega, ; G. A. Petersson, H. N., M. Hada, M. Ehara, K. Toyota, ; R. Fukuda, J. H., M. Ishida, T. Nakajima, Y. Honda, O. Kitao, ; H. Nakai, M. K., X. Li, J. E. Knox, H. P. Hratchian, J. B. Cross, ; V. Bakken, C. A., J. Jaramillo, R. Gomperts, R. E. Stratmann, ; O. Yazyev, A. J. A., R. Cammi, C. Pomelli, J. W. Ochterski, ; P. Y. Ayala, K. M., G. A. Voth, P. Salvador, J. J. Dannenberg, ; V. G. Zakrzewski, S. D., A. D. Daniels, M. C. Strain, ; O. Farkas, D. K. M., A. D. Rabuck, K. Raghavachari, ; J. B. Foresman, J. V. O., Q. Cui, A. G. Baboul, S. Clifford, ; J. Cioslowski, B. B. S., G. Liu, A. Liashenko, P. Piskorz, ; I. Komaromi, R. L. M., D. J. Fox, T. Keith, M. A. Al-Laham, ; C. Y. Peng, A. N., M. Challacombe, P. M. W. Gill, ; B. Johnson, W. C., M. W. Wong, C. Gonzalez, and J. A. Pople, ; Revision E.01 ed.; Gaussian, Inc.: Wallingford, CT, **2004**.

(22)   Bokobza-Sebagh, L.; Zarembowitch, J. *Spectrochimica Acta* **1976**, *32A*, 797-805.

(23)   Wheatley, P. J. *Acta Crystallographica* **1960**, *13*, 80-85.